View metadata, citation and similar papers at core.ac.uk

brought to you by CORE

provided by Digital.CSIC

The free volume of poly(vinyl methylether) as computed in a wide temperature range and at length scales up to the nanoregion

Dušan Rako, S. Capponi, F. Alvarez, and J. Colmenero

Citation: J. Chem. Phys. **134**, 044512 (2011); doi: 10.1063/1.3525380

View online: http://dx.doi.org/10.1063/1.3525380

View Table of Contents: http://jcp.aip.org/resource/1/JCPSA6/v134/i4

Published by the American Institute of Physics.

Related Articles

Stretching semiflexible polymer chains: Evidence for the importance of excluded volume effects from Monte Carlo simulation
J. Chem. Phys. 136, 024901 (2012)

Oxygen and nitrogen plasma hydrophilization and hydrophobic recovery of polymers
Biomicrofluidics 6, 016501 (2012)

Interferometric scanning microscopy for the study of disordered materials
Appl. Phys. Lett. 99, 251912 (2011)

(Electro)mechanical behavior of selectively solvated diblock/triblock copolymer blends
Appl. Phys. Lett. 99, 242901 (2011)

Statics of polymer droplets on deformable surfaces
J. Chem. Phys. 135, 214703 (2011)

Additional information on J. Chem. Phys.

Journal Homepage: http://jcp.aip.org/

Journal Information: http://jcp.aip.org/about/about_the_journal

Top downloads: http://jcp.aip.org/features/most_downloaded

Information for Authors: http://jcp.aip.org/authors

ADVERTISEMENT

Downloaded 10 Jan 2012 to 161.111.180.191. Redistribution subject to AIP license or copyright; see http://jcp.aip.org/about/rights_and_permissions

The free volume of poly(vinyl methylether) as computed in a wide temperature range and at length scales up to the nanoregion

Dušan Račko,[1,2,a)] S. Capponi,[1,3] F. Alvarez,[3,4] and J. Colmenero[1,3,4]
[1]*Donostia International Physics Center, Paseo de Manuel Lardizabal 4, 20018 Donostia-San Sebastián, Spain*
[2]*Polymer Institute, Slovak Academy of Sciences, 842 36 Bratislava, Slovakia*
[3]*Departamento de Física de Materiales, Universidad del País Vasco (UPV/EHU), Apartado 1072, 20080 San Sebastián, Spain*
[4]*Materials Physics Center (MPC), Centro de Física de Materiales (CSIC-UPV/EHU), Apartado 1072, 20080 San Sebastián, Spain*

(Received 3 July 2010; accepted 16 November 2010; published online 24 January 2011)

In the present work, we focus on the free volume evaluations from different points of view, including the aspect of probe sizes, temperature, and cavity threshold. The free volume structure is analyzed on structures of poly(vinyl methylether) prepared by fully atomistic molecular dynamics. At first, the temperature behavior of an overall free volume and a free volume separated into individual cavities is shown. The origin of large free volume cavities is explained. A complex view on the cavity number is provided, while a complicated behavior previously observed is now explained. The number of large cavities remained almost constant with the temperature. Oppositely, the number of small cavities related to the atomic packing changes with temperature in a distinct way for glassy and supercooled regions. The cavity number maxima determine a percolation threshold according to percolation theory. The change in polymer properties with temperature can be related to a percolation of the free volume according to the free volume theory, when proper probe radii ~0.8 Å are used for its observation. A construction of probabilistic distribution of free volume sizes is suggested. The free volume distributions reported here are bimodal. The bimodal character is explained by two different packings—atomic and segmental—forming a prepeak and a main peak on the distribution. Further attention is dedicated to comparisons of the computed free volume sizes and the ortho-positronium (o-Ps) lifetimes. The prepeak of the free volume distribution is probably unseen by o-Ps because of a cavity threshold limit. The effect of the shape factor on the computed o-Ps lifetimes is tested. The quasicavities obtained by redistributing the free volume maintain the ratio of the main dimensions with temperature. Finally, novel data on the cavity environment are provided, while it is suggested how these can be useful with the recent developments in the positron annihilation methods. The coordination number of large cavities with the polymer segments is around 1, as predicted in the free volume theory. Similarly to the percolation and the cavity number, the coordination number exhibits a change when explored by a suitable probe radius ~0.8 Å. The insightful visualizations showed properties of interest investigated within the actual work. © *2011 American Institute of Physics*. [doi:10.1063/1.3525380]

I. INTRODUCTION

The free volume theory is a successful concept for relating various transport, structural, and dynamic properties by a single quantity—the free volume.[1–9] The basic idea of this concept is that a molecular body can move if it has a space to do so. The first principles of the concept were formulated soon after the discovery of the atom, and it was used to explain changes of fluidity in liquids.[1] The free volume theory found its stronger impact in the physics of polymers. Polymers have often identical chemical composition with different sizes of macromolecules for which different mobility can be expected. In early stages, thermodynamic and dynamic properties have been correlated to the free volume quantity as a complementary part to the molecular space. Later on, a generalization based on the behavior of transport properties was also given. An important conclusion was that different polymers have the same properties at the same amounts of the free volume. In these approaches, the free volume rather differed from the so-called empty free volume, which is a complementary part of volume to the van der Waals volumes of molecular bodies (e.g., Ref. 10). In further developments, the free volume was associated to the particular molecular bodies, expecting an excess of free volume to occur when the body leaves its position. Other fundamentals of the theory predict a probabilistic distribution of the free volume sizes. The dramatic change of the properties around the glass transition point has been predicted to have something to do with an onset of the free volume percolation.[9] Despite the great success in relating different physical properties, the free volume theory fails in defining a unified free volume quantity. As such the fundamental free volume measurements, like the free volume numbers, distributions of free volume sizes, percolation and geometry, remain without understanding.

a)Electronic mail: dusan_racko@ehu.es.

 © 2011 American Institute of Physics

Downloaded 10 Jan 2012 to 161.111.180.191. Redistribution subject to AIP license or copyright; see http://jcp.aip.org/about/rights_and_permissions

The intrinsic drawback of the purely theoretical approaches is that, in the best case, they can provide the free volume quantity in an indirect way, as a fitting parameter of a particular model. Hence, the free volume is obtained as a material parameter, which is already correlated with a particular transport, structural or dynamic property; on the other hand, independent partial information for linking between macroscopic properties and a microstructure cannot be extracted. In the last two decades two methods for a direct free volume determination by using very small probes below the size of an atom have been developed. First, the experimental method called positronium annihilation lifetime spectroscopy (PALS) determines the defects in structure based on the annihilation behavior of the positronium particle (e.g., Ref. 11). This particle of subatomic size is very sensitive to the regions of lowered electron density. The free volume amounts are determined here from the positronium lifetimes by using semiempirical quantum mechanical hole-size-to-lifetime correlations. This method suffers from an intrinsic limitation too, since it works as a direct method only under the approximation of assuming a spherical geometry of the free volume cavities. In models considering more complicated geometries of the holes, the approximate shape of cavities must be obtained by other ways. The second method for the direct free volume determination is made by computer simulations. Here, the free volume on well equilibrated structures is determined by means of geometrical analyses.

The current state of art in the free volume studies determines a need for a model or a simulation, which would reproduce all basic features of the free volume according to the classical free volume theory, as well as reproducing the free volume amounts predicted by PALS measurements. Naturally, the modeling studies attempted for reproducing the PALS measurements of the free volume. These studies predicted in general that some portion of small cavities (cavity threshold) are inaccessible for localization of a positronium particle.[12–17] In low density systems, the positronium was predicted to reside in pockets of a risen free volume density—quasicavities.[14,17–19] In our recent work, we have shown that the experimental lifetimes—free volume amounts, respectively—can be obtained within both conditions, neglecting of small cavities, as well as division of the free volume structure into quasicavities. The obtained positronium lifetimes, for annihilation models with different geometries, showed only small differences, which scaled with the ratio of most abundant cavity dimensions.[17] In the present paper, a further insight into the free volume structure is provided. To the best of our knowledge, the paper is a solitary work comparing free volume quantities from PALS and computations in such an extensive way and wide temperature region. The free volume is addressed from various theoretical, experimental, and computational aspects.

II. METHODOLOGY

A. Molecular dynamics simulations

The molecular dynamics simulations were performed in the DISCOVER module of the Materials Studio simulation package by Accelrys.[20–22] The molecules were built from scratch, by initializing coordinates of all atoms. Then the structures were cleaned when the bond lengths and angles were adjusted to their equilibrium values according to hybridization. Next, the forces acting between atoms were treated by attributing the condensed-phase optimized molecular potentials for atomistic simulation studies (COMPASS) molecular force field. COMPASS is a second generation molecular force field suited for simulations of condensed phases. A short molecular dynamics run was performed, while the polymeric chain approached energy minima. Using this configuration of the polymeric chain, the amorphous cell was built by means of the amorphous cell protocol. The protocol is based on an extension of well established methods for generating bulk disordered systems, containing chain molecules in realistic equilibrium conformations.[23] The prepared amorphous cell contained seven polymeric chains. Each of the chains consisted of 100 monomers, giving 7014 atoms in total. The structure was equilibrated under isobaric–isothermal thermodynamic conditions (number of particles, pressure and temperature kept constant within NPT ensemble, using the isotropic stress tensor constraint) at 400 K until the conformational distribution, the box side length and the potential energy fluctuated around constant values. In a next step, the structure was dynamically equilibrated in the canonical ensemble (number of particles, volume, and temperature kept constant). The last structure from this NVT step was used as a starting point for data collection, recording structures every 0.01 ps during molecular dynamics (MD) run of 1 ns. The velocity-Verlet algorithm with a time step of 1 fs was used for the integration of the equations of motion. To control the temperature, instead of a real temperature-bath coupling (Nosé–Hoover or Berendsen thermostat) a velocity scaling procedure with a wide temperature window of 10 K was taken.[24] The structures at lower temperatures were obtained in an analogous way. Starting from the equilibrated structure at 400 K, temperature was lowered by 25 K. After the first run, successive runs of 20 ns, collecting data every 0.5 ps, were carried out until we gained 40 ns trajectories without aging phenomena. Within this procedure, we have obtained seven trajectories from production runs in a temperature range between 400 and 250 K. Each of the trajectories contained 1000 structures for analyses of the free volumes.

B. Free volume evaluations

All free volume data have been obtained as an average of the free volume evaluations over 1000 structures for each temperature. Hence, $\sim 5 \times 10^8$ cubic Ångströms of intermolecular space have been explored within the analyses. As we noted earlier, this approach in evaluating the free volume corresponds to a static approximation, similar to evaluating other structural magnitudes like a static structure factor.

In this work, we use two methods for the free volume computations. At first, the occupiable and accessible volumes with the corresponding surfaces are computed by using the Connolly's semianalytical method for calculation of molecular volumes.[25] The method has been developed during past decades and it is available also in the Accelrys software pack-

Downloaded 10 Jan 2012 to 161.111.180.191. Redistribution subject to AIP license or copyright; see http://jcp.aip.org/about/rights_and_permissions

age adjusted also for calculations under periodic conditions. Thanks to the sophisticated algorithm, the method allows fast calculation of molecular volumes with high precision. In the periodic system, the free volume is obtained as a complementary part to the volume which cannot be occupied by a probe with a given radius.

Until now, there does not exist a modification of the Connolly's method that would be able to distinguish separate cavities and compute their statistical, volumetric, or geometrical measures. For this purpose, we use a method based on the numerical integration in three dimensions. This method in principle provides the same results of free volume amounts when the grid spacing used (or the integration element) is sufficiently small. Since the total free volume amount is obtained as a summation of all the free volume increments, the value of the increment can be corrected to obtain the perfect agreement of the computed volumes from the two methods.

In order to obtain the free volume data related to individual cavities, the free volume is analyzed in several consequent steps. At first, the cubic simulation samples are probed with a probe of a given radius. The samples are probed every 0.5 Å which represents a usual grid spacing used within the free volume studies (e.g., Refs. 15–17, 26, and 27). The positions where no overlaps between the probe and atoms occurred are saved. Next, cavities are constructed. A cavity is here represented by an isolated set of overlapping probes. The probing and cavity construction procedures can be carried out much more efficiently if they are done in subsets or use neighbor lists. The use of the neighbor lists, or the subsets with probes, respectively, led to considerable savings of the computational time, so the analysis performs around 200 times faster than it would have when analyzing the full structure at once.[17]

For small probes, most of the free volume is usually situated in one cavity percolating through the simulation box. Therefore, this cavity is additionally redistributed into quasicavities in order to allow further analyses on the individual free volume cavities. The redistribution is performed based on investigation of local maxima of distances from atoms in the intermolecular space.[14,18,19] The local maxima can be determined easily as a node of the probing grid, for which all surrounding (26) nodes have a smaller distance from atoms. In our approach, however, we used a different way. The local maxima were determined as cavity centers of large cavities, detected by larger probes above a certain probe radius.

As mentioned above, the free volume is computed here by summation of the free volume increments. The summation used the original fast method for the computation of the hard spheres with different radii.[28] Because of the huge increase in the computer capacity, it was possible to perform the summation in one loop from the virtual memory. Hence, the calculations with estimated error of 0.25% could have been performed in fractions of seconds.

Finally, the geometrical parameters of the cavities were computed, based on the calculation of the moments of inertia. Diagonalization of the gyration tensor matrices were performed by using a FORTRAN routine LAPACK 3.0.[29] More details on the computation method can be found in our previous works.[15–17]

III. RESULTS AND DISCUSSION

A. The specific volumes

Prior to computation of the free volume data, the atomic structures had to be computed. The structures were obtained by simulated cooling employing the molecular dynamics simulations. Within the cooling, the temperature was decreased by a given temperature step and the structures were annealed in the NPT statistical ensemble as described in the methodology section. Hence, the first volumetric data come from the NPT simulation and are related to the simulated density. The overall volume of the box is shared by the molecular bodies and the empty space. In further investigations, we split the empty space into regions occupiable by probes of given radii. Figure 1(a) shows the temperature dependence of the specific volume of the simulated poly(vinyl methylether) (PVME). The computed specific volumes are compared to the experimental values. The comparison implies a good reproduction of the experimental densities.[30] The deviation ranged from 0.2% in high temperature liquid to around 0.7% at 300 K. At 275 K, the temperature dependence of the specific volume seems to change the slope. This temperature is believed to be a counterpart to the experimental dilatometric glass transition temperature. The shift of the glass transition temperature is a result of the dynamic arrest, and the agreement with the experimental values cannot be obtained in practically feasible computational times. The shift of the glass transition temperature (of the order of ~30 K) is typically encountered in molecular dynamics simulations and may reach several tens of degrees, see, for example, Refs. 15 and 31.

The graph also shows the temperature dependence of the empty space volume computed on the simulated structures. This dependence demonstrates that the empty space follows the dependence of the overall volume. The thermal expansion coefficient of the free volume is slightly smaller from the coefficient for the total volume in liquid. The total difference in slope is 8×10^{-6} giving the deviation of 1.2%. The similar behaviors of the empty space and total volumes confirm that the volume of molecular bodies changes only a little with the temperature. This observation also determines the necessity of a good agreement between the simulated and experimental

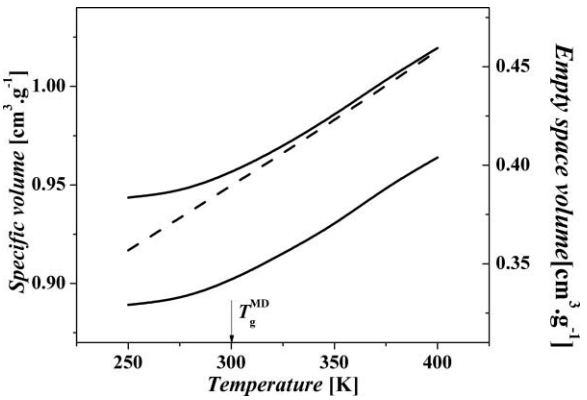

FIG. 1. A comparison between the experimental dilatometric volume and the specific volume obtained from the molecular dynamics simulation (top curve). The dashed line corresponds to the experimental data. The graph also shows the computed portions of the empty space volume (bottom line).

Downloaded 10 Jan 2012 to 161.111.180.191. Redistribution subject to AIP license or copyright; see http://jcp.aip.org/about/rights_and_permissions

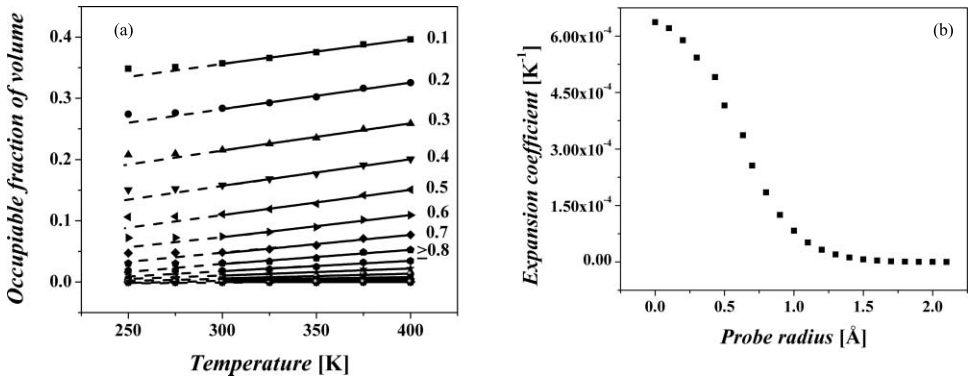

FIG. 2. (a) The free volume fractions computed for different probe radii. The actual probe radii used to calculate the fraction are indicated by the line, with a number which corresponds to the units of Å. The dashed lines correspond to the region where the dependence deviates from the linear behavior due to the shift of the simulated *T*g. (b) The dependence of the expansion coefficient computed for the particular probe radius.

specific volumes, since all additional volume would transfer to the free volume.

The fraction of the empty space at simulated glass temperature T_g^{MD} is 35.7%. This amount is close to the value 36% predicted by the packing fraction for the random packing of hard spheres.[32] The packing fraction as the complementary property of the empty space can be higher for the random packings of spheres with different radii.[33] Taking into account that the interaction potential describes the atoms as soft spheres, the packing in the simulated structures is far from its maxima and large free volume vacancies can be expected.

Figure 2(a) shows the fractions of free volumes occupiable by probes with given nonzero radii. The free volume determined by a spherical probe with a nonzero radius corresponds to the empty space between the molecular bodies minus some portion of geometrically excluded volume. The computed free volume data at the given temperature and the probe radius are shown with symbols. The data points in the region above T_g^{MD} which we suppose that properly reproduce the liquid region are also described by linear fits. The fitting analysis confirms the linear dependence of the free volume with the temperature in agreement with the free volume theory.[4] Moreover, the linear dependence is observed independently of the used probe radii. Slight deviations of the computed free volume data are observed below the assumed glass transition temperature T_g. This deviation is apparent for all investigated probes. On the numerical data, we could observe also that for large probes above some radius the temperature dependence starts from zero at certain temperature. The reason is that occupiable regions, large enough to contain the probe, start to occur only above some temperature as the molecular structure expands.

Another interesting feature is the change in slope of the temperature dependences of occupiable volumes. This feature also can be observed on the free volume dependences reported in an earlier work,[34] although it was not discussed there. The slope of the dependence decreases with the increasing probe radii. As a result, the ratio of the volume shared by larger and smaller cavities changes. This may lead to an intriguing conclusion that the free volume changes on the account of the large cavities, by processes such as the flowing of molecular bodies into larger cavities and splitting them into smaller regions. Although this picture is not to be entirely dispelled within the article, we can demonstrate that the creation of new free volume amounts occupiable at first by small probes is more probable. The situation is well illustrated in Fig. 2(b), showing the thermal expansion coefficient for the occupiable volume as a function of the probe radius. We can observe that the coefficient decreases with the probe radius displaying the curve as a "sigmoidal-like" shape. The expansion of the free volume occupiable by smaller probes follows more closely the expansion of the total volume of molecular structure. The largest change in thermal expansion coefficient occurs for probes between 0.5–0.9 Å. The more intense change can be related to another process starting to act on the free volume—the formation of individual cavities (see Sec. III D). Later, the change in slope stabilizes with larger probes again. This picture may also imply that most of the free volume starts to exist as the interstitial volume. The changes in the separated free volume cavities arise from the change in the overall free volume more likely than directly from a change in the specific volume.

B. Accessible and occupiable volume

In this section, a different view on the occupiable free volume is shown. The occupiable volume is discussed as a function of the probe radius and also in relation to the so-called accessible volume. In Fig. 3(a) the dependence of the probe occupiable volume from Fig. 2(a) is redrawn as isotherms and shown as a function of the probe radii for four temperatures from our investigated range. The dependences start at the value corresponding to the empty space fractions and steeply decrease as the probe radii become larger. The dependence of the free volume starts to deviate from the steep decrease at the large probes where the existence of the free volume cavities is assumed. This behavior is to be considered now as general as it can be seen on the free volume data computed for atomistic simulations, such as polybutadiene[35] or amorphous sucrose.[26] In these works, the deviation from the steep descent declines at around 0.5 Å as shown also for our case in Fig. 3(a). For probes larger than 1.0 Å less than 1% of the volume can be occupied by a probe. The

Downloaded 10 Jan 2012 to 161.111.180.191. Redistribution subject to AIP license or copyright; see http://jcp.aip.org/about/rights_and_permissions

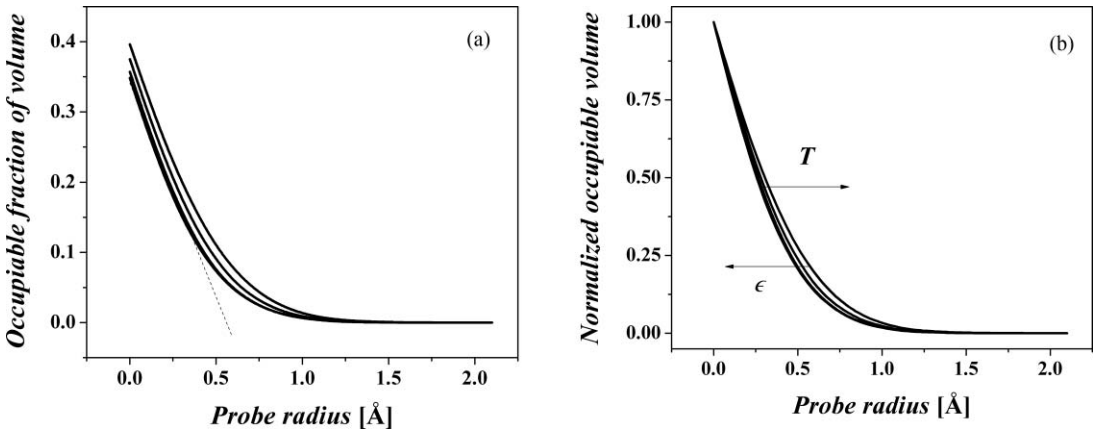

FIG. 3. (a) The fractions of occupiable volume as a function of the probe radii computed for different temperatures. The lines correspond from bottom to 250, 300, 350, and 400 K. The dashed line is a lead to indicate the deviation from the steep descent. (b) The fractions of occupiable free volume normalized to a point probe. The arrows indicate the direction in which the temperature T or hardness $\in$ increase.

dependence always ends with a jump because of the finite size of the probe. It may not be obvious from the graph because of the low amounts of the occupiable volume fraction. Similar dependences were computed also for coarse grain simulations for polyethylenes,[34] polypropylene,[36] and a polycarbonate,[37] naturally, the free volume disappears at larger probe radii predicted as the result of larger distances between the grains.

The shape of the dependence is a unique feature itself. Just consider the simplest picture on the free volume vacancies in the matrix, when the free volume consists of spherical cavities with a constant radius. Then the occupiable volume would remain constant up to the radius of such the cavities, where it would drop to zero. For a more complicated state, when the cavities are represented by probabilistic distributions an s-shaped dependence should be preserved. On the other hand, the shape of the dependence can be well described by an exponential decay function (with a squared correlation coefficient $R^2 = 0.995$). The mathematical meaning of the exponential decay is that a constant probability acts on all population per unit of an independent variable. For our case, the population would be represented by free volume elements and the independent variable is the probe radius. The exponential decay dependence may suggest that in a larger system (statistical ensemble) even larger cavities than detected here can develop spontaneously.

The relation between the occupiable volume and the probe radius can be given based on the concentric shell model.[38] The derivation of the model resulted into exponential equations, which in generalized form correspond to those for the exponential decay. The model also relates other variables such as the bead (atom) radii, the density, and hardness. The hardness is a measure of mutual penetrability of the beads or atoms. The parameter of hardness changes from 1, for completely nonpenetrable spheres, to 0 for spheres, which can be placed randomly. As shown earlier,[35] the dependence of the occupiable free volume fraction in molecular structures from atomistic simulations occurs closer to the second limit case. Additionally, by comparing the curves normalized to a point probe computed for several temperatures, we may see that the predicted hardness parameter decreases with rising temperature, Fig. 3(b). The randomness in this case increases more likely due to the higher configurational freedom than due to a higher penetrability of molecular bodies.

C. The free volume surface

In this section, we report on the surface areas computed for the occupiable volumes for different probe radii. The variation of the surface areas with the temperature and probe radius has more complicated behavior than it is in the case of the occupiable volume. As shown in Fig. 4(a) the surface area in general increases with temperature. The intensity of the increase changes differently for different probes. The surface corresponding to the empty volume changes less intensively. The areas computed in the periodic box are smaller than the areas computed on the same molecules, but placed separately in vacuum. The area in such case was around 9 $\times$ 10^3 Å^2 higher (20%). The difference arises from the overlaps of the atoms in the simulated packings of molecules. The specific surface computed as surface area per unit volume in Fig. 4(b) shows a continuous increase up to 300 K. Above this temperature the specific surface may drop for probes close to van der Waals radii. Furthermore, we may see that the surface area rises the most rapidly for the probe radii from the region where the breaking of the free volume structure into isolated cavities is supposed. Figures 4(c) and 4(d) show the computed slopes characterizing the increase of the surface area with the temperature for a given probe radii. Figure 4(c) represents a simplified case, when the computed surface areas were fitted by a linear equation. This simplified picture is to demonstrate the characteristic shape of the curve. As compared to Fig. 2(b), we may observe that the surface area rises with the highest slopes in the region where the more intensive changes in the free volume are reported. Despite the expansivity of the free volume, where the linear dependence is predicted by the free volume theory, no such prediction is made for the expansion of the surface area. Therefore, fitting analyses with more complicated functional forms would be suitable. For this case, we fitted the data presented in Fig. 4(a) by

Downloaded 10 Jan 2012 to 161.111.180.191. Redistribution subject to AIP license or copyright; see http://jcp.aip.org/about/rights_and_permissions

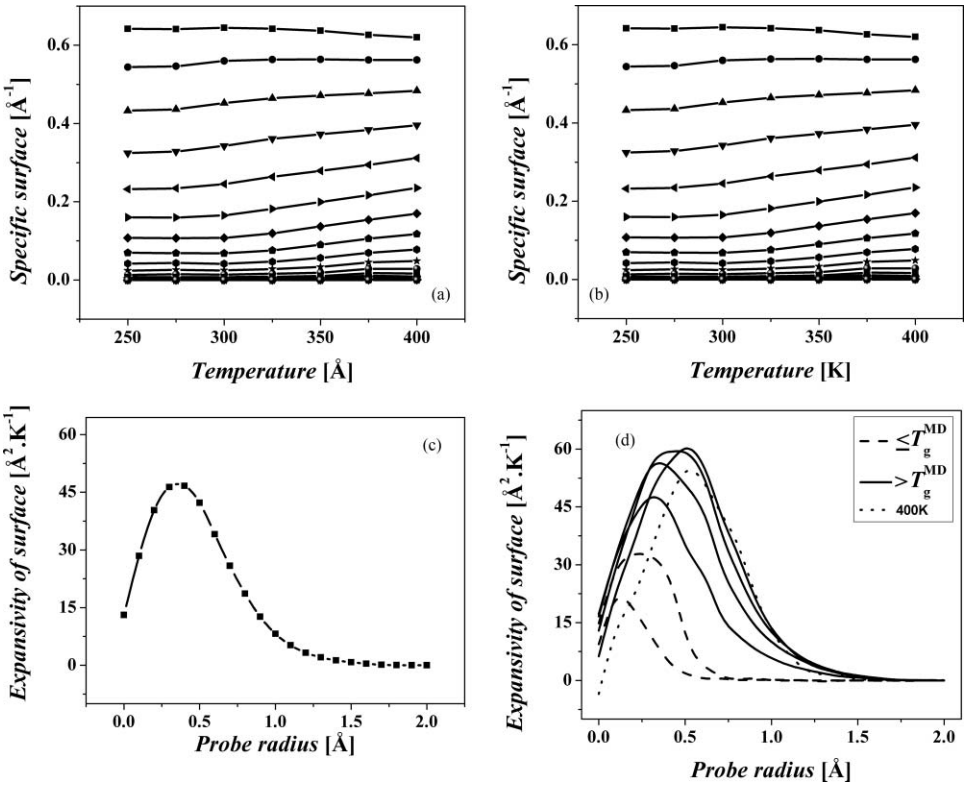

FIG. 4. (a) The total surface areas computed with probes of different radii and at different temperatures. (b) The specific surface area computed from the total surface areas relating them to the total volume of the box. The corresponding radii start from 0 Å for the top line and increase by 0.1 Å. (c) The expansivity of the cavity surface for different radii, computed as a slope of a linear fit over the total surface areas and (d) The expansivity of the cavity surface for different radii, computed as a slope at given probe radii of a polynomial fit over the total surface areas.

a simple polynomial (cubic) function. Next, we computed the slopes as the first derivations at given temperature. Figure 4(d) shows the computed slopes as isotherms dependent on the probe radii. Again we may observe that the peak of the surface expansion occurs between 0.3–0.8 Å, corresponding to the region of the steep decrease in Fig. 2(b). In this region, the free volume structure splits in the individual cavities. We may also observe that the overall change in the surface area (which could be an integral of a particular curve) is smallest below the "glass transition from simulation" and it drops again at 400 K where the true liquid phase is assumed.

D. The cavity number

In Secs. III A–III C, we have already provided a certain insight into the formation of individual cavities in the free volume structure. Based on this picture, we may expect that the number of cavities will exhibit a complicated behavior too. In an earlier work, the number of cavities computed for two distinct probe radii were reported.[34] The computed numbers of cavities for the two probes showed qualitatively different behavior, although the authors did not comment on the observed behavior. In a recent work,[17] some of us computed the number of cavities as a function of the probe radius. As we observed, the computed distribution showed a peak placed around the probes with radius ~0.7 Å. The existence of such a maximum is very natural now. As the probe radius increases, the free volume structure breaks into isolated cavities. Because the occupiable volume changes too, the occupiable (probe accessible) sites are depleted soon and the cavity drops again. The position of the peak is situated in the region where the form of the free volume, from a percolated space into individual cavities, is observed. Let us note that within the cavity constructions by using a discrete probing grid the percolation of cavities may change slightly, and the position of the peak may slide to smaller values when finer grid spacing is employed.[39]

In Fig. 5(a) we show that such distributions develop at all temperatures. However, the position of the peak will slightly shift with temperature to higher values. This is consistent also with Fig. 3(b), which infers that at higher temperatures the cavity breaking starts at higher probe radii. The distributions were computed starting from probe radii of 0.4 Å. The reason is that the computational costs heavily increase with decreasing the probe radii toward a point probe. However, the question whether there can exist also a cavity for a point probe with zero radius, can be answered that, in principle, it is possible. The molecular structure consists of finite-size spheres; hence, in a proper coordination of atoms, a free space can be formed between them. Due to the huge computational costs, we do not investigate the physical meaning of this presumption further.

When the distributions in Fig. 5(a) are redrawn as a function of temperature, the origin of the qualitatively different behavior for various probe radii is obvious [see Fig. 5(b)]. We may classify the behavior of the cavity number with the

Downloaded 10 Jan 2012 to 161.111.180.191. Redistribution subject to AIP license or copyright; see http://jcp.aip.org/about/rights_and_permissions

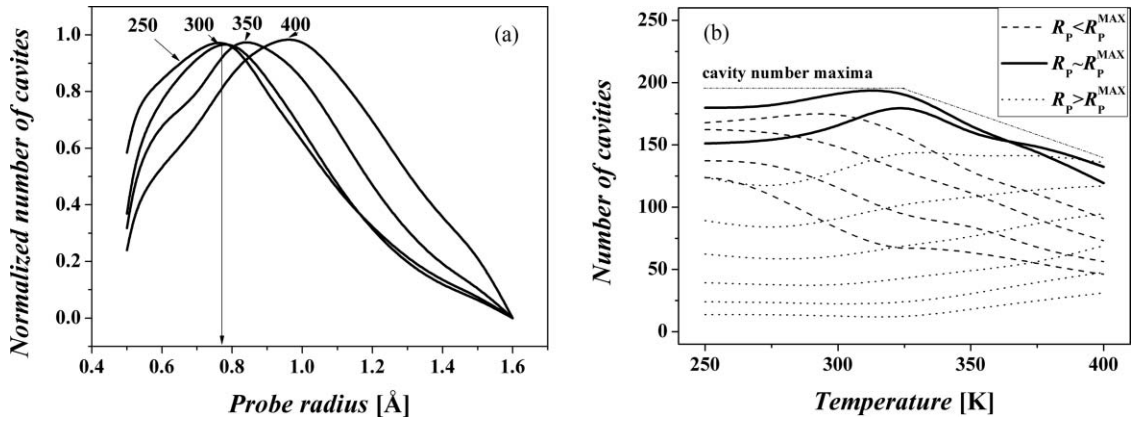

FIG. 5. (a) The distribution of the cavity number as a function of the probe radii computed at different temperatures. The corresponding temperatures are indicated with lines in units of K. (b) The graph shows a different view on the same data. The cavity numbers are plotted as a function of temperature for given radii. The number of cavities for the small probes is indicated by dashed lines. The rising numbers of cavities, computed for large probes are shown by dotted lines. The solid lines were computed for the probe radii around the position of the cavity number maxima. These lines exhibit a presence of maxima. The graphs explain the nature of the complicated behavior of the cavity number.

probe radii into three groups. For the small probe radii below the peak of the cavity number, the total number of cavities will decrease with temperature. We may describe this behavior on the temperature as merging of the small cavities into one mostly percolated cavity. On the other hand, for the large probes new occupiable regions are created, so the number of cavities increases. Finally, from the view on the cavity number distributions presented in Fig. 5(b) it is also clear now that for some probe radii the system will be passing through a maximum with rising temperature. This behavior will be typical for probe radii around the position of the cavity number maximum. Figure 5(b) also indicates the dependence of the total maxima of the cavity number. This maximum can be a result of interplay between different packings—atomic and the packing of molecular bodies. The maximum of the cavities seems to develop a global maximum between 325 and 350 K. Another interesting feature is the drop of the cavity number maxima with the temperature. As we have seen in Fig. 3(d) at the higher temperature the cavities are created at higher probe radii. At the higher probe radii, the free volume can be divided into fewer cavities.

E. The free volume distributions and the percolation

The classical free volume theory assumes two fundamental properties of the free volume. One is a probabilistic distribution of the free volume element sizes.[9] The other one is the percolation of the free volume elements. Within the percolation theory an important prediction is made, that at the point where the percolation occurs a dramatic change in properties is observed.[40] It is now natural, that since the first computational works the authors have been attempting to show the distribution functions of the free volume. However, a typical shape of the free volume distribution computed by the direct probing approach showed bimodal or trimodal distributions.[13,18,19,34,37,39] In these distributions the highest occurrence of the small cavities was observed, followed by a considerable lower number of cavities in the intermediate range. On some distributions also a large cavity is observed which usually percolated the simulation box.

Note that in some other approaches to the free volume simulation, like Voronoi or Delaunay tessellations, the probabilistic distributions of the free volume sizes are regularly observed. However, the free volume amounts determined by the tessellations are not clear, at least for polydisperse systems. This is because in a fully atomistic simulation the indices and vertices of the polyhedra are function of both, the free volume sizes as well as the atomic radii. The percolation of the Voronoi or Delaunay polyhedra[37,41] has also been observed, although the authors reported that no change of the properties around the percolation point has been observed.[42]

In Figs. 6(a) and 6(b) we show integral distributions of volume as a function of cavity volume and temperatures. The distributions are normalized by relating the distributions to the absolute amounts of the occupiable free volume at the given temperature. Furthermore, the figures provide data computed for two probe radii from the interval where the peak of the cavity number distributions is observed. We can see the distributions change as a function of the temperature as well as probe radii. For small probes, or a point probe respectively, the free volume structure should be percolated. For large probes, a narrow distribution of the cavity volumes is observed. The percolation of the free volume structure can be traced by probe radii around the position of the cavity number maxima [Fig. 5(a)]. This is in an agreement with the percolation theory, which says that around a percolation threshold a maximum should occur.

The percolated cavity may represent a real puzzle in simulations. From the aspect of free volume analyses, the percolation complicates analysis of the cavity structure. The evaluations of the basic free volume measurements, like the cavity number, cavity volume, and the cavity geometries, apply only on individual cavities. In the case of the percolated cavity a bias from the simulated box sizes may take place. The problem of percolating cavity might not be encountered in dense systems, such as hydrogen bonded liquids, even for small probes around radius of 0.5 Å.[15] This is because even

Downloaded 10 Jan 2012 to 161.111.180.191. Redistribution subject to AIP license or copyright; see http://jcp.aip.org/about/rights_and_permissions

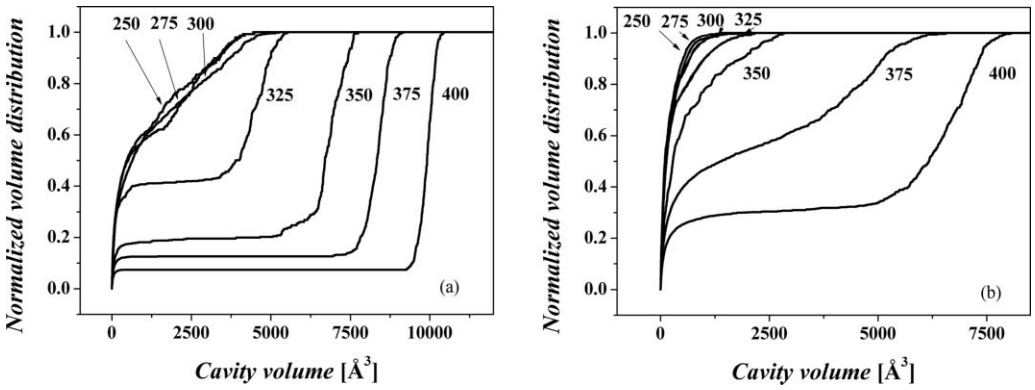

FIG. 6. (a) and (b) The integral distributions of the free volume computed at different temperatures. The corresponding temperature is indicated with a number by the lines in units of K. The shown distributions are computed for two probe radii 0.7 and 0.9 Å. The distributions are normalized by relating to the total amount of the free volumes.

the smaller probe radii were larger than the radius belonging to the cavity number maxima. However, in a later investigated polymer system we coped with the problem of the percolating cavity. In order to break the cavity into quasicavities, we have redistributed the free volume structure around the local maxima of the free volume occurrence as suggested in earlier works.[14,17–19] Such maxima can be determined as probing positions for which all 26 neighboring nodes have lower distance from atoms. These criteria, however, can be too tight and may lead to splitting even bulky cavities according to subtle irregularities, which could be associated to the level of a cavity surface. As a result, the distributions of the cavity sizes may occur around lower values. In our approach, we determined local maxima in a different way. The local maxima were given as centers of large cavities determined by larger probe radii. The probe radii used were close above the position of the cavity number maxima (Fig. 5). This approach also allows scaling the position of the peak of the free volume sizes distribution.

As it has been reported in earlier works, and as we show in Fig. 7, the former delta wing shaped distribution [Fig. 7(a)] of the free volume changes after the redistribution into the probabilistic distribution [Fig 7(b)]. Now, the origin of the probabilistic distribution can be explained by the distribution of the cavity centers in the sample volume. As we have shown in our recent work,[17] based on the cavity—cavity radial distribution function the distribution of the large cavities in space is completely random, contrary to small cavities, for which a certain pattern has been detected. Now consider that the free volume structure is redistributed around the centers of these large cavities. Finally, the distribution of the free volume observed here is bimodal. We suggest that the bimodal character of the distribution is given by two different packings in the structure. One is related to the atomic packing, the other originates from the packings of the whole polymer segments on a scale of Kuhn segments.

Moreover, we may remark that the procedure of the free volume redistribution is in its principle familiar with the Voronoi or Delaunay tessellations (e.g., Ref. 43). However, in this case instead of atoms, the volume is associated to the random points corresponding to centers of large cavities and only free volume part of space is considered. It can scale to larger free volume structures too (for example determining coordination or percolation of the large cavities). Finally, let us note that the percolation phenomena predicted by the free volume theory[9] should be explored also on larger scales, where a percolation of the larger free volume formations should be examined. At small scales on the level of atoms, the percolation can be hidden in the primary formation of cavities based on the probe geometry as shown in Secs. III A–III D.

F. Cavity shape

The next property of the free volume evaluated is the cavity geometry. The cavity geometry can be evaluated in a discrete way by computing the main axes of the ellipsoid of inertia. The ellipsoid of inertia represents a momentum distribution of probes forming the cavity.[44] Another common way to expressing the geometry is computing a surface-to-volume ratio. The previous geometrical evaluation of the cavity geometry showed that the irregularities expressed as asphericity, acylindricity,[35,44] or statistical deviations like variance and uniformity increase with the volume of cavities.[13] In our recent work, we compared the match of the cavity geometry with several basic geometrical shapes.[17] Here, we provide further view on the cavity geometry computed for different probes and temperatures. At first, the side-to-length ratios of the main axes of the ellipsoid of inertia are computed and based on these ratios the histograms of occurrence are created. In Fig. 8 we show the histograms computed for two temperatures from our temperature range of interest, by using four probes 0.53, 0.9, 1.1, and 1.5 Å. We may see that for the smallest one no stable distribution is observed. It is because most of the free volume is situated in a percolated cavity and only casual individually existing free volume cavities appear in the structure. For larger probes, the percolated structure starts to fall apart into individual cavities. Here, a probabilistic distribution of the side-to-length ratios can be observed centered about a characteristic ratio 0.6:1.0. For larger probes, the values of the side-to-length ratios around unity become frequented because even the large cavities can contain only single probes. We may see that the main features observed on histograms are shifted with temperature so that the same features occur for a smaller probe at lower temperature. In

Downloaded 10 Jan 2012 to 161.111.180.191. Redistribution subject to AIP license or copyright; see http://jcp.aip.org/about/rights_and_permissions

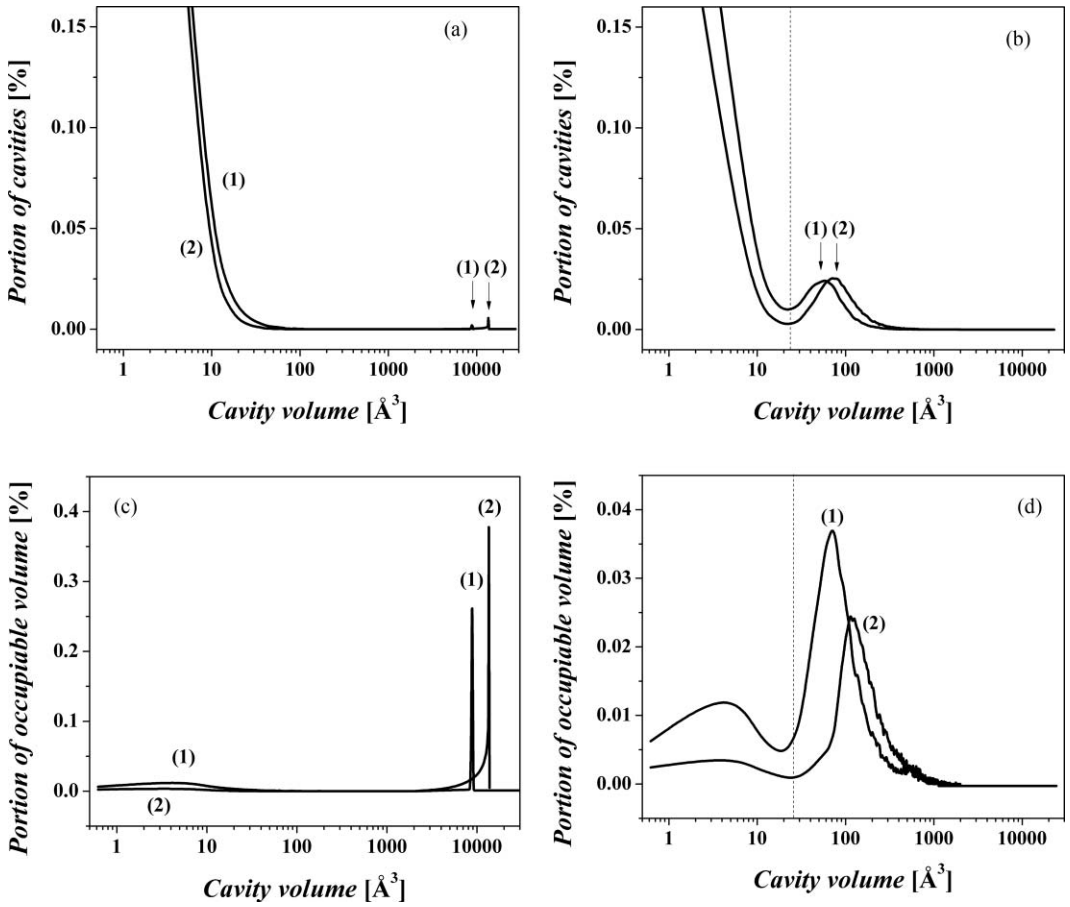

FIG. 7. Distributions of cavity numbers and volumes for two temperatures 300 (1) and 400 K (2), represented as a portion of cavities, by normalizing to the overall cavity numbers or the total free volume, respectively. Graph (a) shows the normalized distribution of the volume computed for a probe with radius R_P = 0.53 Å. The distribution starts with a steep descent corresponding to single probe cavities. Arrows show the percolated cavities. Graph (b) shows the distribution of the cavity number after redistributing the free volume structure into the quasicavities. The dashed line shows where we put cavity threshold limit. Graph (c) shows the distribution of the free volume in terms of the cavity sizes. Before redistribution of the microstructure into quasicavities, the major part of the volume is situated in percolated cavities. Graph (d) shows the distribution of the quasi-cavity sizes.

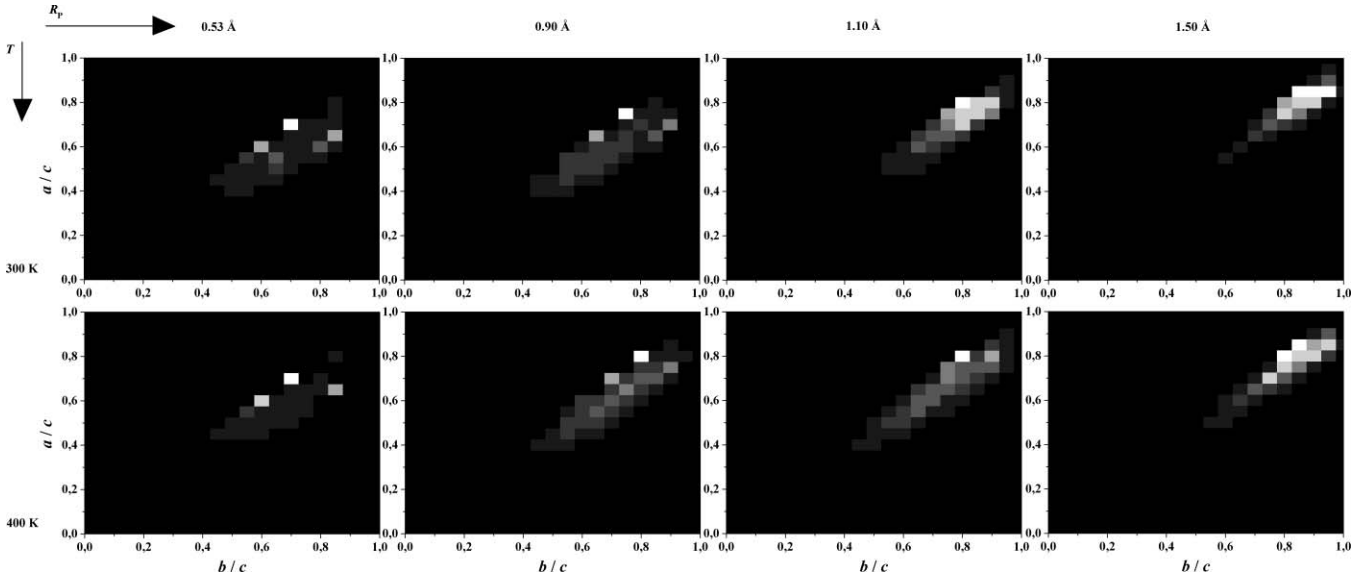

FIG. 8. Distribution of the side-to-length ratios of the axes of the ellipsoid of inertia. The brighter gray tones correspond to a higher frequency of occurrence of computed ratios. The most abundant single probe cavities, with the ratios 1:1 are not shown.

Downloaded 10 Jan 2012 to 161.111.180.191. Redistribution subject to AIP license or copyright; see http://jcp.aip.org/about/rights_and_permissions

principle, this shift follows the shifting of the cavity number maxima with the increasing temperature [Fig. 5(a)]. The geometrical dimensions computed on the quasicavities keep a constant value of the match to a simplified geometrical representation, as well as the side-to-length ratios, within the temperature range investigated (81% for cylinder). The variation of the matching with the temperature was within the boundaries of the standard deviation. Figure 9 shows the geometrical features discussed above in a different view, as surface-to-volume ratios. The graph shows that the ratio computed for the empty space by a zero point probe slightly decreases with increasing temperature. For the zero point probe, the area of the free volume cavities corresponds to the van der Waals surface of the molecules. The decrease occurs because at the higher temperatures the molecules get separated and more of the molecular space is accessible to the probe. The decrease of the surface to volume ratio has been already manifested by the specific area (Fig. 4). The ratios start to increase with increasing the probe radius reaching a maximum. The maximum occurs approximately in the region of the cavity formation and slightly shifts toward large probes with the increasing temperature. For very large probes, the data become unstable and the computed values occasionally provide the side-to-length ratios corresponding to a sphere with the given probe radius. An apparent global maximum of the surface-to-volume ratio computed for 350 K can be a result of two factors: the largest surface-to-volume ratios are obtained for isolated mid-sized cavities (Fig. 8) and the occurrence of a global maximum of cavity number close to 350 K [Fig. 5(b)].

G. The computed free volume cavities and the PALS

In a consecutive step, the computed free volume sizes or the positronium lifetimes can be compared to the experimentally obtained values. In our comparison we will show the positronium lifetimes rather than volumes, since the positronium lifetime is the quantity directly obtained from the PALS experiment. The input data for the positronium lifetime computations are the cavity volumes and dimensions computed within the free volume analyses. The corresponding lifetimes are calculated based on the lifetime-to-volume semiempirical

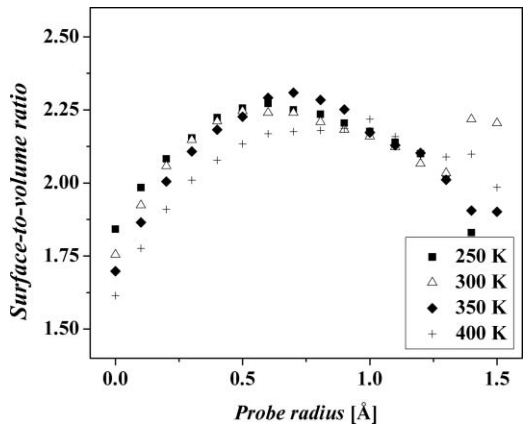

FIG. 9. The overall surface to volume ratio of the free volume computed for four characteristic temperatures from our investigated temperature region.

quantum mechanical correlations. In the experimental determination of the free volume, the same equations are used to calculate the cavity sizes from the positronium lifetimes. In extension to the experimental determination, we also use the model with enhanced assumption of the cylindrical geometry and use the cavity dimensions obtained within the geometrical analyses.

In previous studies of the high free volume systems, it has been suggested that probes with small radii can be too sensitive to provide the picture of the cavity structure.[45] As we have shown, the number density of cavities can be reproduced by using the larger probes with radii around 1.0 Å; however, the free volume dropped dramatically. Therefore, within the free volume determination we used a small probe with radius of an ortho-positronium (o-Ps) atom, $R_P = 0.53$ Å, and additionally redistributed the percolated free volume structure as suggested in related works.[14,18,19] However, the determination of the local maxima in the original approach may be too tight and leads to predicting smaller cavities around 2–3 Å of hole-size equivalent radii.[27] In our approach we determine the cavity maxima in a different way, as centers of cavities determined by larger probes with radii close above to the cavity number maxima. As suggested from our recent work, by changing probe size criteria, the positronium lifetimes can be obtained in a span between those of percolated structure to those computed on quasicavities.[17] Naturally, in the case of larger cavities the role of the shape factor becomes more important, decreasing the computed lifetimes. In order to obtain the experimental values, small cavities below some threshold volume should be discarded. In Fig. 10(a) we show that the overall cavity number drops with temperature, consistently with what was already observed in the low molecular systems.[15,16] The overall number of cavities corresponds to the number of large cavities obtained from redistribution of the free volume, plus a larger cavity number sampled by very small probes. When eliminating cavities with certain small volumes, the cavity number in the temperature region below ~350 K remains constant. As shown previously,[17] these small cavities could correspond to some subtle structural feature sampled along the atomic structure of the polymeric chain and they are not accessible to o-Ps atom localization. As we have also shown in Figs. 3 and 7 in this work, this structural feature can be sampled particularly by small probes at sizes, where the fractal division of the interstitial space occurs. Consistently with the distributions in Fig. 7, the amount of the small cavities to be neglected drops with the increasing temperature. The number (density) of holes is often assumed to be related to the relative intensity of an o-Ps signal during annihilation measurements.[46,47] On the other hand, some other experimental works argued that the intensity of the annihilation signal has a more complicated origin, showing that the intensity is affected by light of a particular wavelength or chemical composition.[48] Understanding the origin of the relative intensity can enhance amount of unique information obtain by the PALS measurements. As the computational approach of the free volume analyses provides also information on the cavity number, a direct comparison with the relative intensity is afforded. Figure 10(a) plots the relative intensity on the right *y*-axis versus the normalized temperature. Despite scat-

Downloaded 10 Jan 2012 to 161.111.180.191. Redistribution subject to AIP license or copyright; see http://jcp.aip.org/about/rights_and_permissions

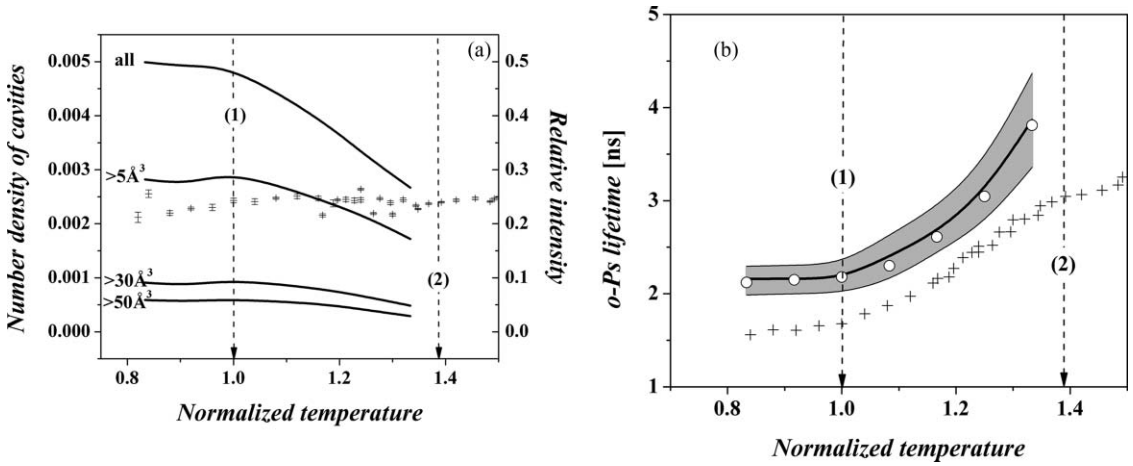

FIG. 10. A comparison of computed (solid lines) and experimental (+ symbols) data. The arrows show the glass transition temperature (1) and the onset of a plateau in PALS (2). Graph (a) The graph shows the number density of cavities as a function of the normalized temperature and cavity threshold given in cubic Ångströms. The graph also shows relative intensities from o-Ps lifetime experimental measurements. Graph (b) The comparison of the ortho-positronium lifetimes as computed from spherical model (open circles), cylindrical model (gray area), and experimental data (+ symbols). The values for the spherical model were computed for cavity threshold of 30 Å^3. The solid lines representing the values from the cylindrical model are computed for 40, 50, and 60 Å^3.

tered values at high temperature above $1.2T_g$, the dependence of the relative intensity seems to have a slightly increasing trend. However, the total difference is smaller than 9% in the investigated temperature region. The slightly increasing trend is, however, comparable with the increasing trends of larger cavities [Fig. 5(b)]. This could be consistent with an assumption that o-Ps atom localize in larger cavities. The number of computed quasicavities obtained after redistribution of the free volume seems to preserve this trend $(0.8–1.0)T_g$. A use of larger probes to determine cavity centers for the free volume redistribution could even pronounce the increasing trend of computed values. On the other hand, as the observed variation of the relative intensity as well as computed cavity numbers show only slight variations with the temperature, the assumption of a constant cavity number given in some models for the free volume fractions (Ref. 49) is fairly satisfied too.

Figure 10(b) compares the experimental data from PALS measurements[50] to computed values. The computations involved two models considering different geometries. One is the most simplified and the most common model for spherical holes.[51–53] The second cylindrical model[54] was shown to reproduce the PALS data when considering a geometrical representation of cavity closest to the real cavity shape.[17] We prefer comparing lifetimes because the o-Ps lifetime is the actual quantity directly obtained by the PALS experiment. The computed and experimental data are normalized to corresponding glass transition temperatures observed in the PALS experiment $T_g^{PALS} \cong 250$ K,[50] or obtained in the molecular dynamics simulations $T_g^{MD} = 300$ K (Fig. 1). The gray area between solid lines corresponds to the values computed by cylindrical model, with thresholds of cavity volumes between 40–60 Å^3. The thick line is computed for 50 Å^3. The lifetimes computed by using the spherical model are represented by open circles. In the case of the spherical model, idealized geometry provides an overestimate of cavity lifetimes;[17,55] hence, a smaller cavity threshold of 30 Å^3 had to be considered. From the comparison between the computed values, we may see that after using different cavity thresholds to compensate the overestimates of values between models, the values keep the same temperature dependence. The reason for this can be that overall geometrical parameters represented by the ratio of the main dimensions of cavities do not change (significantly) with temperature as discussed in Sec. III F. The computed data qualitatively agree well with the experimentally measured lifetimes up to the onset of plateau region. The plateau region is not reproduced what indicates that the origin of the plateau observed in the experiment cannot be explained only by the shape factor of the cavities. Quantitatively the computed o-Ps lifetimes for a given cavity threshold are longer than the experimental values. After scaling the graph by normalizing to the corresponding glass transition temperature, the data showed roughly constant difference in the investigated temperature region up to the onset of the plateau. This is quite clearly the result of large cooling rate which causes the structure to freeze at higher amounts of the free volume.[15,16]

H. The cavity environment

In our previous work, we have investigated the cavity environment in terms of the cavity–cavity radial distribution functions. The distributions showed a prepeak occurring at small separations or detected by small probes, respectively. We have suggested that this peak may correspond to some structural feature sampled along the polymeric chain. In the present work, we furthermore provide an investigation of the cavity environment. From the experimental point of view, the PALS has been shown to have the ability to detect chemical environment for particular chemical elements. However, the existing data are rare and exist for only a few chemical systems.[56,57] Hence, no particular comparison of experimental results is done here, and rather we show the ability of providing such kind of information by the simulation approach too.

Downloaded 10 Jan 2012 to 161.111.180.191. Redistribution subject to AIP license or copyright; see http://jcp.aip.org/about/rights_and_permissions

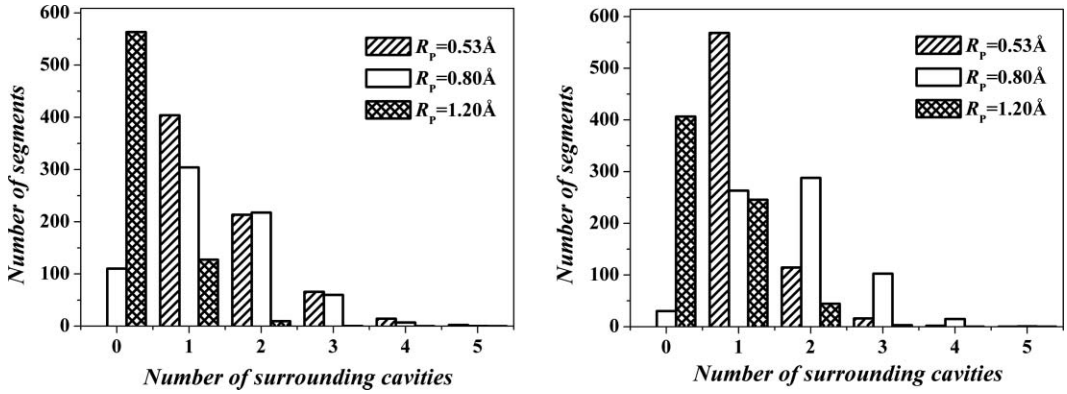

FIG. 11. Histograms show portions of polymeric segments (from total 700) coordinated by a particular number of cavities. The graphs are shown for two temperatures 300 and 400 K, and the data were computed as an average over 1000 structures for the given temperature and particular probe radius.

In Figure 11, the histograms enumerating the numbers of cavities neighboring to each of 700 polymer segments in the simulated structures are shown. Two limit cases are analyzed from our investigated temperature range. The data were averaged over 1000 structures. The graphs infer that the small probe, with the radius 0.53 Å, is a very sensitive probe to which all segments are accessible during probing. However, for the probes with larger radii there are a considerable number of inaccessible regions. This number is decreased as the structure opens with the increasing temperature. In the case of the small probe, the number of segments detected to be surrounded by only one cavity increases. It is because of spread-

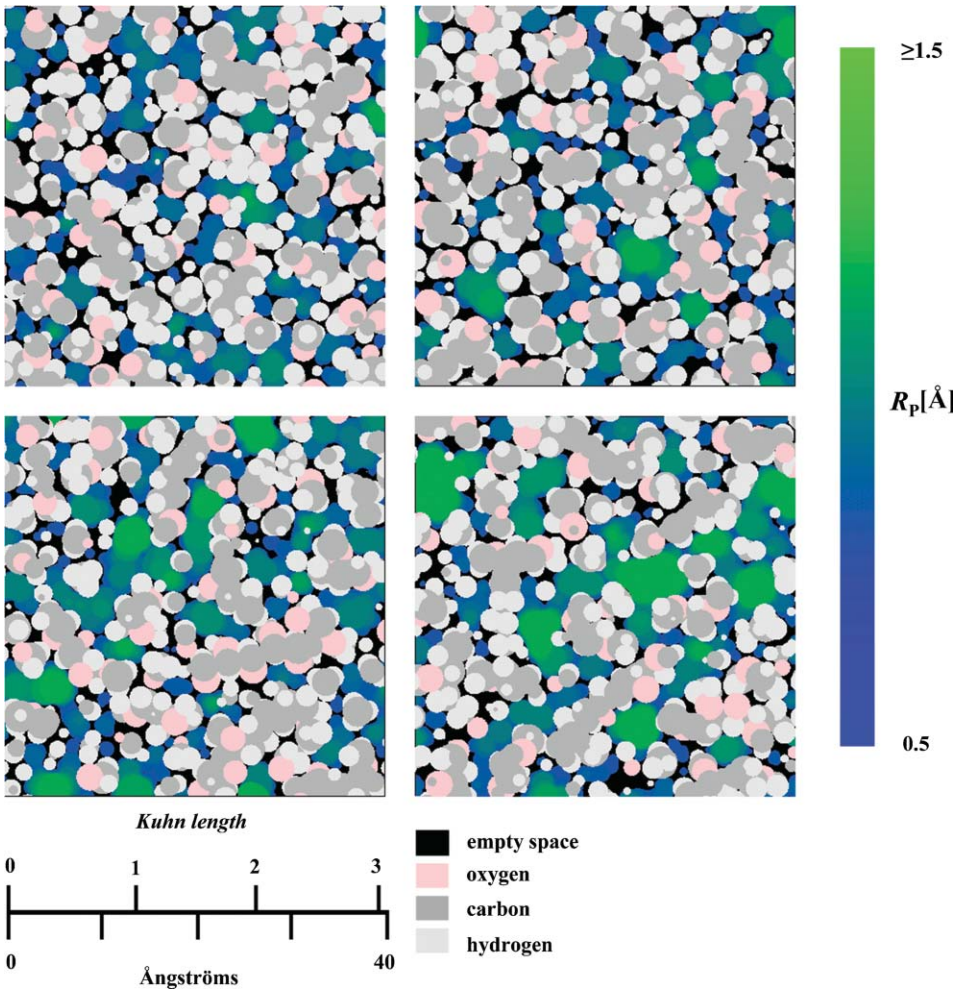

FIG. 12. The free volume structure has been shown as a slice for 250, 300 (top row), 350, and 400 (bottom row) K. The green regions represent large free volume regions accessible to probes with large radii. Black regions represent interstitial volume probed by very sensitive probes with radii below the percolation threshold $R_P < 0.5$ Å. The pictures show also the chemical environment of the free volume cavities. Two length scales in units of Å as well as Kuhn lengths (for PVME ~ 13 Å) (Ref. 58) are shown for reference.

Downloaded 10 Jan 2012 to 161.111.180.191. Redistribution subject to AIP license or copyright; see http://jcp.aip.org/about/rights_and_permissions

ing of the percolated cavity. We may, further, observe that rather large number of segments participates in formation of more than one cavity. This may occur in the case of small single-probe cavities. As we suggested earlier,[17] this portion of small cavities sample some subtle feature, in principle represented by the interstitial volume. For larger cavities, even represented by a single probe of 1.20 Å, associating of a polymer segment by more than one cavity becomes unlikely.

A complex view on the object of our investigation in this work is given in Fig. 12 by representative visualizations. The visualizations show slices of the molecular structure together with the free volume cavities. The visualizations are provided for four characteristic temperatures from our investigated range. Cavities with large free volume amounts accessible to larger probes are distinguished by a color scale from blue to green. Probes with radii below 0.5 Å are considered to be able probing the intermolecular space in detail. This space, however, would correspond to the interstitial volume and no cavity formation is supposed here. This detailed space is shown in black color. In the actual slice, we may observe that only a few really large cavities can be found. These cavities may have approximately size on a scale of Kuhn segments. Within the centers of these large cavities the free volume has been associated, producing the probabilistic distributions of the cavity sizes (see Sec. III E). Redistributing of a free volume sampled by more sensitive probes increases the cavity surface, and it is responsible for the complicated cavity shape generally computed in previous geometrical investigations.[17,35,37,39,43] In agreement with the previous study the elongated cavity shape can be remarked.

IV. SUMMARY AND CONCLUSIONS

We have investigated free volume structure at different temperatures starting from a point probe. The temperature dependences of the free volume fractions computed for different probes show linear dependence on temperature. The thermal expansion coefficient of the free volume drops with increasing temperature as the free volume fractions computed for larger probes are a function of both, density and the probe geometry.

The dependence of the free volume with increasing probe radius follows an exponential behavior. This describes how large defects develop from the disordered atomic structure spontaneously. The bending on the exponential curve is related to the formation of individual cavities. The bending can distinguish the free volume existing in two different forms. The region of the steep drop of the occupiable volume is associated with depletion of large amounts of probing sites and corresponds to a percolated free volume. This part of the intermolecular space can be characterized with a fractal division of space. The region below the bending represents a free volume existence as individual cavities, which have larger geometrical freedom for probing. Further, comparison with the concentric model shell infers decrease of hardness of the molecular structure with rising temperature. The randomness or disorder of the structure can be related to the developing of larger cavities. The formation of cavities, as change of the character of the free volume, reflects on different properties evaluated, such as temperature dependences of the occupiable volume, cavity numbers, specific surface, or geometrical parameters. The cavity formation is also reflected by the dependence of the free volume quantities on a probe size, such as the occupiable volume, occupiable-to-accessible volume ratios, thermal expansivity of free volume, expansivity of surface, shifting of cavity number distributions, or producing probabilistic distributions.

The complicated and qualitatively different behavior of the cavity number computed for small and large probes was explained. Additionally, the maximum was observed to shift slightly with increasing temperature. Hence, for certain probe radii around the position of the cavity number maxima the system was observed to be passing through a cavity number maximum also with increasing temperature. The cavity number increases or drops with temperature according to the position of the cavity number maximum. In the same time, the cavity number maximum characterizes a percolation threshold value in the primary cavity formation/free volume percolation. This percolation is not necessarily connected with the dramatic change of physical properties predicted by the classical free volume theory. An approach for investigation of larger free volume formations and examining their percolation over the structure with the change of the physical properties was suggested.

The distributions of the cavity numbers and volumes show polymodal distributions in percolating structures. Probabilistic distributions were produced by redistributing the free volume around local maxima of the free volume occurrence. A modified way for obtaining these maxima as centers of large cavities prevented bulky cavities from crumbling. The procedure is similar to construction of space tessellations. The distributions of the free volume produced in this way are bimodal. The bimodal character of the distributions is natural and can originate from two different packings—atomic and segmental.

The geometry of cavities was evaluated by side-to-length ratio of the main axes of ellipsoid of inertia and by the surface-to-volume ratios for different probes and temperatures. The evaluations show that the same features are computed at higher temperatures when larger probes used. The behavior follows the shift of the position of the cavity number maxima and the percolation threshold. The geometrical dimensions computed on the quasicavities keep a constant value in the temperature range investigated. The variation of the geometrical evaluations computed on quasicavities with the temperature was within the boundaries of the standard deviation. The evaluations can be important from the aspect of the classical free volume theory, supposing that a constituent can move if it has a space to. The slightly flat-shaped geometry with side-to-length ratio 1:2 suggest that for most molecular probes including the polymer segments the constituents in structure will affect the structure and produce their own free volume. From the aspect of the semiempirical PALS models with enhanced geometry, the constant ratio of the geometrical dimensions predicts that the data from spherical model will be overestimated by a constant difference value.

The comparison with the PALS data showed that experimental values of the ortho-positronium lifetimes/cavity volume can be obtained under two assumptions: (i) cavities

Downloaded 10 Jan 2012 to 161.111.180.191. Redistribution subject to AIP license or copyright; see http://jcp.aip.org/about/rights_and_permissions

below certain threshold volume are not able to localize positronium atom, (ii) the free volume structure is redistributed into quasicavities. In the low temperature region, the computed lifetimes increase with a smaller slope; however, our glassy region is probably shifted to higher temperatures. The shift is due to some scale effects, such as cooling rate or box sizes employed. The comparison has also showed that the shape factor is not sufficient to explain the plateau, which seems to be observed in experiments at higher temperatures. Underestimate of the lifetime values in the mid-region of temperatures could be compensated by rearranging the free volume around even bigger cavities. It may suggest that the cavity centers of longest persisting cavities should be determined upon some dynamic criteria.

The evaluation of the cavity environment demonstrates the ability of the computational approaches in the free volume evaluations to be used as a complementary tool in the exploration of the free volume environment suggested by recent developments in the experimental method. The computed data show that a probe with 0.53 Å is a sensitive probe able to access all polymer segments. In the case of larger probes only segments around larger free volume cavities can be associated. In some case a polymer segment can be associated with more than one cavity. This happens mainly in the case of the probes with the radii around the position of the cavity number maxima or percolation threshold, respectively.

For a direct visual examination of the properties investigated in this work a complex visualizations has been prepared, showing the free volume regions in color scale according to the probe size used. In the same picture, the molecular bodies forming the polymer are shown and the atoms are distinguished based on their chemical origin.

ACKNOWLEDGMENTS

This work was supported by Project No. MAT2007–63681 (Spanish Ministry of Education) and Grant No. IT-436–07 (Basque Government). Support from Spanish Ministry of Education Grant No. CSD2006-53 is also acknowledged. We also thank D. Cangialosi for providing us with PALS unpublished results of PVME.

[1] A. J. Batschinski, Z. Phys. Chem. **84**, 643 (1913).
[2] T. G. Fox and P. J. Flory, J. Appl. Phys. **21**, 581 (1950).
[3] A. K. Doolittle, J. Appl. Phys. **22**, 1031 (1951).
[4] T. G. Fox and P. J. Flory, J. Phys. Chem. **55**, 211 (1951).
[5] M. L. Williams, R. F. Landel, and J. D. Ferry, J. Am. Chem. Soc. **77**, 3701 (1955).
[6] D. H. Cohen and D. Turnbull, J. Chem. Phys. **31**, 1164 (1959).
[7] D. Turnbull and M. H. Cohen, J. Chem. Phys. **34**, 120 (1961).
[8] D. Turbull and M. H. Cohen, J. Chem. Phys. **52**, 3038 (1970).
[9] G. S. Grest and M. H. Cohen, Adv. Chem. Phys. **48**, 455 (1981).
[10] A. J. Kovacs, Fortschr. Hochpolym.-Forsch. **3**, 394 (1964).
[11] W. Brandt and A. Dupasquier, *Positron Solid State Physics* (North-Holland, Amsterdam, 1983).
[12] R. M. Dammert, S. L. Maunu, F. H. J. Maurer, I. M. Neelov, S. Niemelä, F. Sudholm, and C. Wästlund, Macromolecules **32**, 1930 (1999).
[13] C. Nagel, E. Schmidtke, K. Gunter-Schade, D. Hofmann, D. Fritsch, T. Strunskus, and F. Faupel, Macromolecules **33**, 2242 (2000).
[14] D. Hofmann, M. Heuchel, Y. Yampolskii, V. Khotimskii, and V. Shantarovich, Macromolecules **35**, 2129 (2002).
[15] D. Račko, R. Chelli, G. Cardini, J. Bartoš, and S. Califano, Eur. Phys. J. D **32**, 289 (2005).
[16] D. Račko, R. Chelli, G. Cardini, S. Califano, and J. Bartoš, Theor. Chem. Acc. **118**, 443 (2007).
[17] D. Račko, S. Capponi, F. Alvarez, J. Colmenero, and J. Bartoš, J. Chem. Phys. **131**, 064903 (2009).
[18] D. Hofmann, M. Entrialgo-Castano, A. Lerbret, M. Heuchel, and Y. Yampolskii, Macromolecules **36**, 8528 (2003).
[19] M. Heuchel, D. Hofmann, and P. Pullumbi, Macromolecules **37**, 201 (2004).
[20] S. W. Bunte and H. Sun, J. Phys. Chem. B **104**, 2477 (2000).
[21] H. Sun, J. Phys. Chem. B **102**, 7338 (1998).
[22] J. Yang, Y. Ren An-min Tian, and H. Sun, J. Phys. Chem. B **104**, 4951 (2000).
[23] D. N. Theodorou and U. W. Suter, Macromolecules **18**, 1467 (1985).
[24] J. Colmenero, F. Alvarez, and A. Arbe, Phys. Rev. E **65**, 041804 (2002).
[25] M. L. Connolly, J. Am. Chem. Soc. **107**, 1118 (1985).
[26] V. Molinero, T. Çağin, and W. A. Goddard III, Chem. Phys. Lett. **377**, 469 (2003).
[27] J. C. Jansen, M. Macchione, E. Tocci, L. De Lorenzo, Y. P. Yampolskii, O. Sanfirova, V. P. Shantarovich, M. Heuchel, D. Hofmann, and E. Drioli, Macromolecules **42**, 7589 (2009).
[28] R. Voorintholt, M. T. Kosters, G. Vegter, G. Vriend, and W. G. J. Hol, J. Mol. Graphics **7**, 243 (1989).
[29] LAPACK driver routine version 3.0, University of Tennessee, University of California Berkeley, NAG Ltd., Courant Institute, Argonne National Lab, and Rice University, 1999.
[30] T. Shiomi, F. Hamada, T. Nasako, K. Yoneda, K. Imai, and A. Nakajima, Macromolecules **23**, 229 (1990).
[31] R. Chelli, P. Procacci, G. Cardini, R. G. Della Valle, and S. Califano, Phys. Chem. Chem. Phys. **1**, 871 (1999).
[32] J. Bernal, Proc. R. Soc. London **280**, 299 (1964).
[33] W. Schaertl and H. Sillescu, J. Stat. Phys. **77**, 1007 (1994).
[34] D. Rigby and R. J. Roe, Macromolecules **23**, 5312 (1990).
[35] S. Misra and W. Mattice, Macromolecules **26**, 7274 (1993).
[36] V. M. Shah and S. A. Stern, and P. J. Ludovice, Macromolecules **22**, 4660 (1989).
[37] S. Arizzi, P. H. Mott, and U. W. Suter, J. Polym. Sci., Part B: Polym. Phys. **30**, 415 (1992).
[38] P. A. Rikvold and G. Stell, J. Colloid Interface Sci. **108**, 158 (1985).
[39] S. J. Marrink, R. M. Sok, and H. J. C. Berendsen, J. Chem. Phys. **104**, 9090 (1996).
[40] J. W. Essam, Rep. Prog. Phys. **43**, 833 (1980).
[41] M. L. Greenfield and D. N. Theodorou, Macromolecules **26**, 5461 (1993).
[42] F. W. Starr, S. Sastry, J. F. Douglas, and S. C. Glotzer, Phys. Rev. Lett. **89**, 125501 (2002).
[43] W. Brostow, J. P. Dussault, and B. L. Fox, J. Comput. Phys. **29**, 81 (1978).
[44] E. Schmidtke, K. Gunter-Schade, D. Hofmann, and F. Faupel, J. Mol. Graphics Modell. **22**, 309 (2004).
[45] M. Rudel, J. Kruse, K. Rätzke, F. Faupel, Y. P. Yampolskii, V. P. Shantarovich, and G. Dlubek, Macromolecules **41**, 788 (2008).
[46] Y. Kobayashi, W. Zheng, E. F. Meyer, J. D. McGervey, A. M. Jamieson, and R. Simha, Macromolecules **22**, 2302 (1989).
[47] Y. Y. Wang, H. Nakanishi, Y. C. Yean, and T. C. Sandreczki, J. Polym. Sci., Part B: Polym. Phys. **28**, 1431 (1990).
[48] Y. C. Yean, P. E. Mallon, and D. M. Schrader, *Principles and Applications of Positron and Positronium Chemistry* (World Scientific Publishing Co. Pte. Ltd, Singapore, 2003).
[49] G. Consolati, M. Levi, L. Messa, and G. Tieghi, Europhys. Lett. **53**, 497 (2001).
[50] D. Cangialosi *et al*. (unpublished).
[51] H. Nakanishi, S. J. Wang, and Y. C. Jean, in *Positron Annihilation Studies of Fluids*, edited by S. C. Sharma (World Scientific, Singapore, 1988), p. 292.
[52] S. J. Tao, J. Chem. Phys. **56**, 5499 (1972).
[53] M. Eldrup, D. Lightbody, and J. N. Sherwood, Chem. Phys. **63**, 51 (1981).
[54] B. G. Olson, T. Prodpran, A. M. Jamieson, and S. Nazarenko, Polymer **43**, 6775 (2002).
[55] V. P. Shantarovich, J. Polym. Sci., Part B: Polym. Phys. **46**, 2485 (2008).
[56] Q. Deng, S. Sung, T. Mahmood, G. M. Zhou, X. Lu, S. Y. Shen, K. L. Cheng, E. W. Hellwuth, C. F. Tsai, Y. C. Jean, and M. F. Lou, Mater. Sci. Forum **105**, 1541 (1992).
[57] G. Dlubek, H. M. Fretwell, and M. A. Alam, Macromolecules **33**, 187 (2000).
[58] G. A. Schwartz, D. Cangialosi, A. Alegria, and J. Colmenero, J. Chem. Phys. **124**, 154904 (2006).

Downloaded 10 Jan 2012 to 161.111.180.191. Redistribution subject to AIP license or copyright; see http://jcp.aip.org/about/rights_and_permissions